Charles University
Faculty of Science

Study programme: Chemistry

Branch of study: Chemistry

Jan Stoklasa

The role of boron oxide in oxidative dehydrogenation of hydrocarbons

Role oxidu boritého při oxidativní dehydrogenaci uhlovodíků

Bachelor´s thesis

Supervisor: Mgr. Miroslav Rubeš, Ph.D

Prague, 2023

Prohlašuji, že jsem tuto bakalářskou práci vypracoval(a) samostatně a výhradně s použitím citovaných pramenů, literatury a dalších odborných zdrojů. Tato práce nebyla využita k získání jiného nebo stejného titulu.

Beru na vědomí, že se na moji práci vztahují práva a povinnosti vyplývající ze zákona č. 121/2000 Sb., autorského zákona v platném znění, zejména skutečnost, že Univerzita Karlova má právo na uzavření licenční smlouvy o užití této práce jako školního díla podle §60 odst. 1 autorského zákona.

I declare that I carried out this bachelor thesis independently, and only with the cited sources, literature and other professional sources. It has not been used to obtain another or the same degree.

I understand that my work relates to the rights and obligations under the Act No. 121/2000 Sb., the Copyright Act, as amended, in particular the fact that the Charles University has the right to conclude a license agreement on the use of this work as a school work pursuant to Section 60 subsection 1 of the Copyright Act.

In Prague, date 22. 5. 2023 .....

Jan Stoklasa
Author's signature

I would like to thank Mgr. Miroslav Rubeš, Ph.D. for many helpful discussions about my thesis, introducing to linux and quantum-chemistry programs and specially for commenting the thesis.

Also, I would like to thank to all my family members for their support and motivation.

Title: The role of boron oxide in oxidative dehydrogenation of hydrocarbons

Author: Jan Stoklasa

Department: Department of Physical and Macromolecular Chemistry

Supervisor: Mgr. Miroslav Rubeš, Ph.D., Institute of Organic Chemistry and Biochemistry of the Czech Academy of Sciences

Keywords: boron oxide h-BN reaction mechanism oxidative dehydrogenation catalyst characterization

Contents

1. Introduction

The light alkenes (olefins) are often used in chemical industry as precursors to synthesis of more complex molecules and many other tasks. Hundreds of tons of olefins are produced worldwide, with 160 million tons of propylene and 115 million tons of butylene in 2019 [1]. There is a growing trend in both their production and consumption, indicating that the demand for these substances is expected to continue increasing in the coming years. The "convention" catalysts for oxidative dehydrogenation (ODH) are based on transition metals [2], such as vanadium. Nowadays, non-metal catalysts are being studied, e.g. porous hexagonal boron nitride (h-BN) due to its high selectivity towards olefine production and low CO_2 content [3].

Currently propane dehydrogenation process (DH) covers approximately 10% of propylene production. However, DH processes have several disadvantages, such as their endothermic nature, equilibrium limits, and frequent catalyst regeneration [4]. Oxidative dehydrogenation (ODH) of alkanes to olefins should be an alternative to DH, which solve its main problems.

Transition metal oxides are the most commonly studied catalysts in ODH processes, but their selectivity to olefins decreases with increasing alkane conversion. First metal free catalysts were carbon-based nano particles, e.g. carbon nanotubes. [5]. In 2016 the Hermans group discovered interesting activity of h-BN catalyst in ODH reaction, which opened new possibilities for research and it could be a way to reduce environmental impact of production of light alkenes [6]. Boron-based catalysts have gained recognition as promising materials in ODH processes due to their high selectivity and reduced production of carbon oxides.

The main challenge in establishing ODH process of the light alkanes is prevent further oxidation of prepared alkene (e.g. propylene) to more thermodynamically stable carbon oxide and carbon dioxide. The vanadium oxide catalyst is suitable conventional catalyst for ODH process, nevertheless the propylene selectivity typically drops to less than 60% at 10% propane conversion, making the ODH process with conventional catalysts unprofitable. In the experimental work described in the Grant et al. studies [6] the direct comparison between vanadium oxide, h-BN and boron nitride nanotubes (BNNT) catalyst were made. The catalysts based on boron nitride presented an impressive selectivity with higher conversion. The h-BN catalyst reaches 79% of propylene selectivity at 14% propane conversion which contrasts with conventional V/SiO_2 catalyst that reach 61% propylene selectivity at only 9% propane conversion. The h-BN catalyst also produce significantly less of carbon oxides - comparing 9% of CO_x selectivity for h-BN catalyst and 33% for conventional one. According their research the main secondary product of ODH reaction of propane with vanadium catalyst is carbon monooxide, instead of ethene for h-BN, which is also valuable product that can be further utilized. In case of h-BN catalyst the combined propylene and ethylene selectivity is 91%. They also verified, that the h-BN catalyst remains stable and with similar activity for at least 32 hours. In contrast, h-BN surfaces exhibits a high stability under pure oxygen atmosphere (i.e., oxidative conditions), thus

it is surprising that the h-BN surface is catalytically active at all.Due to the observed differences in the dependencies of the reaction rate on the partial pressure of oxygen and propane, it is likely that an alternative reaction mechanism is involved, distinct from that known in conventional vanadium catalysts. In the research they also characterized material before and after the ODH reaction. The analysis of a spent catalyst have shown an increasing amount of oxygen in h-BN surface. The same increase was not observed after surface treatment with air at same temperature (490°C), that indicated required presence of propane and oxygen mixture to activate the h-BN surface. [6]

In the early 1960s, Knox published [7] his experimental data, which suggested that O2H radicals play an important role in the ODH process of propane. The temperature of propane and oxygen mixture was elevated to 591K to avoid mixture ignition and composition of products was analyzed. Note, that the product composition to certain degree reflects the results of ODH process on h-BN catalysts. Thus, it is highly likely the radical mechanism plays an important role in the ODH on non-metal catalysts such as h-BN [8].

As per the findings presented in Hongping's paper [9], the catalyst surface edges play a key role in the ODH process. Based on their calculations the *zig-zag* boron edge was found to have higher activity for adsorbing O_2 molecules compared to the boron-terminated *zig-zag* edge or armch-chair edge.

In Jinshu's research [3] the experiments involving isotopically labelled oxygen molecules indicated non-dissociative adsorption of O_2 at BOx sites, which could prevent the oxygenation of alkanes and alkenes through oxygen radicals. Furthermore, upon introduction of propane to the reacting mixture, immediate observation of mixed oxygen isotopes ($^{16}O^{18}O$) in the reaction mixture indicated dissociation of the adsorbed oxygen molecule with the assistance of propane. The similar behavior was also reported in h-BN surface catalyst [10]. After replacement of propane with propylene in the reaction mixture, the presence of oxygen ($^{16}O^{18}O$) molecules was not observed, indicating no interaction between absorbed oxygen and propylene on the surface. According to Jinshu's paper this fact is the cause for the high selectivity of boron based catalyst in ODH process.

According to the findings from the experiment on the ODH process of ethane it was predicted that h-BN catalysis exhibits stability under the ODH process conditions [11]. The study demonstrated that even after subjecting the h-BN catalyst to 200 tests, the B-OH edge groups remained unaffected. Furthermore, peaks associated with characteristic stretches of B-OH edge groups were observed at approximately 3400 cm^{-1} . The catalyst exposure to only ethane atmosphere caused no changes in observed band position of the OH groups and also no ethane conversion was detected. After addition of molecular oxygen to the reaction mixture the reaction of OH edge groups with the molecular oxygen are indicated due to the visible lowering of intensity of the OH vibrational bands. The intensity of the vibration was recovered after steam re-activation. The isotopic labelled experiments have shown no reaction between labelled surface B-OD/H and molecular oxygen based on no detection of species with H or D atom. Additionally, no chemical interaction between labelled surface and ethane was observed,

which show that edge by itself is cause C-H bond activation. In contrast, ethylene and H_2O and also the HDO and D_2O were generated immediately with decreasing trend in their production after beginning of treatment with reaction mixture of molecular oxygen and ethane. That show the exchange of H atom between ethane and hydroxyl group in catalyst surface edge, considering these surface as active place of the catalyst. According to their kinetic experiments dependence on oxygen concentration correspond with the mechanism controlled by O_2 activation on catalyst surface. The direct reaction of ethane with oxygen species on the catalyst surface can be suggested by second order dependency on ethane concentration. According their DFT calculation they predict present of two radicals $BNO^{\bullet}$ and $HO_2^{\bullet}$ which have the role in ODH process in studied system.

The BNNT catalyst can be also used for dehydration of methanol. According to Esrafili's research the methanol molecule can be absorbed to BNNT catalyst surface. It shows that the boron based catalyst can be used in more dehydrogenation task then ODH process of propane. [12]

According to the review article [1], despite significant shift in research in recent years, there is a missing spectroscopic evidence pertaining to the key intermediate that is necessary for a fully understanding of ODH process.

2. Methods

2.1 Density Functional Theory

Density Functional Theory (DFT) is a widely used computational approach in quantum chemistry and material modelling. DFT is based on the fundamental premise that the electronic properties of a system can be described by the electron density, which is a function of the spatial coordinates and spin. In contrast, the *standard* wave functions based method (e.g. Hartree-Fock) depending on spatial coordinates and spin each individual electron. DFT ground state energy is thus determined by electron density functional (vide infra) [13].

2.1.1 Electron density

Electron density is a probability to find one electron of arbitrary spin at an infinitesimal element of space. Integration electron density ρ over all space $\boldsymbol{r}$ gives us the total number of electrons N:

$$\mathrm{N} = \int \rho(\boldsymbol{r}) d\boldsymbol{r} \tag{2.1}$$

The obvious corollary of equation 2.1 is that the electron density reaches zero when the electron is at the infinite distance from the nucleus:

$$\lim_{\boldsymbol{r}\to\infty} \rho(\boldsymbol{r}) = 0 \tag{2.2}$$

According to the fact, that nuclei can be considered as a point charge, we can expect that there are local maximums of electron density at these Also, the atomic number can be also identified by electron density dependence, where for the nuclei A which is located in the maximum of electron density $\boldsymbol{r}_\mathrm{A}$ follows:

$$\left.\frac{\partial \bar{\rho}}{\partial r_\mathrm{A}}\right|_{r_\mathrm{A}=0} = -2\mathrm{Z}_\mathrm{A}\rho(\boldsymbol{r}_\mathrm{A}) \tag{2.3}$$

where Z_A is a atomic number of atom A, r_A is a radial distance from atom A and $\bar{\rho}$ is the spherically averaged density.

These properties fix the Hamiltonian of a system (within Born - Oppenheimer approximation), i.e, number of electrons, positions and charges of atoms.

2.1.2 Early approach to original DFT

Energy can be divided into kinetic and potential components. The potential energy, which is a function of electron density, can be easily determined if the system behaves classically. The interaction between electron (density) and nuclei is defined as follows:

$$V_{\mathrm{ne}}(\rho(\boldsymbol{r})) = \sum_{i}^{nuclei} \int \frac{\mathrm{Z}_i}{|\boldsymbol{r} - \boldsymbol{r}_i|} \rho(\boldsymbol{r}) d\boldsymbol{r} \tag{2.4}$$

and repulsion between two electron densities is determined in order to optain formula for:

$$V_{\mathrm{ee}}(\rho(\boldsymbol{r})) = \frac{1}{2} \iint \frac{\rho(\boldsymbol{r}_1)\rho(\boldsymbol{r}_2)}{|\boldsymbol{r}_1 - \boldsymbol{r}_2|} d\boldsymbol{r}_1 d\boldsymbol{r}_2 \tag{2.5}$$

The kinetic energy, a model called homogeneous electron gas (jellium) proposed. It is a system of infinitely number of electrons which are moving in infinitely volume, where the positive charge is uniformly distributed. This homogeneous electron gas has a constant non-zero density. Thomas and Fermi in 1927 describe kinetic energy of the system by following equation:

$$V_{\mathrm{ueg}}(\rho(\boldsymbol{r})) = \frac{3}{10}(3\pi^2)^{\frac{2}{3}} \int \rho(\boldsymbol{r}_2)^{\frac{5}{3}} d\boldsymbol{r} \tag{2.6}$$

The equations for kinetic and potential energy (Eq. 2.4 - 2.6) depend on the electron density, which is already a function of spatial coordinates. According to the mathematical definition of a functional, which is a function, which takes a function as its argument and returns a scalar value, the terms for kinetic and potential energy are also functionals.

Although these equations demonstrate the basic principles of the DFT approach; these equations are only approximate and they are not used nowadays in chemistry calculation. The equation 2.5 is using very crude approximation for the electron-electron repulsion term, disregarding the energy changes associated with electron correlation and exchange. This approximation can be improved by the concept of "hole function".

$$\langle \Psi | \sum_{i<j}^{\text{electrons}} \frac{1}{r_{ij}} | \Psi \rangle = \frac{1}{2} \iint \frac{\rho(\boldsymbol{r}_1)\rho(\boldsymbol{r}_2)}{|\boldsymbol{r}_1 - \boldsymbol{r}_2|} d\boldsymbol{r}_1 d\boldsymbol{r}_2 + \frac{1}{2} \iint \frac{\rho(\boldsymbol{r}_1)h(\boldsymbol{r}_1;\boldsymbol{r}_2)}{|\boldsymbol{r}_1 - \boldsymbol{r}_2|} d\boldsymbol{r}_1 d\boldsymbol{r}_2 \tag{2.7}$$

The first term in equation 2.7 is classical electron-electron repulsion term from the equation 2.5, the second term corrects the first one using the hole function h, which is related to electron density ρ. The notation $h(\boldsymbol{r}_1;\boldsymbol{r}_2)$ means that the hole function is centered at the position of electron 1 and in general h is function of only $\boldsymbol{r}_2$.

In 1950s Slater published how to reduce calculation time based on fact, that exchange hole is larger than correlation hole. Slater suggested update the former form by approximating the exchange hole as a sphere of constant potential depending electron density in that position. The exchange energy in this model follows:

$$E_{\text{ex}}(\rho(\boldsymbol{r})) = \frac{-9\alpha}{8}\left(\frac{3}{\pi}\right)^{\frac{1}{3}} \int \rho^{\frac{4}{3}}(\boldsymbol{r}) d\boldsymbol{r} \tag{2.8}$$

where, constant $\alpha = 1$. The following empirical calculation have shown, that $\alpha = \frac{3}{4}$ produce more accurate results. This DFT approach is not as commonly used in modern DFT calculation, but it is still used for some inorganic chemistry problems.

The theory presented so far is much easier compared to wave-function-based models. However, this approach produces significant errors, so initially, this method did not have a significant impact in theoretical chemistry. In the 1960s, Hohenberg and Kohn/Sham modified the DFT theory, which caused DFT to become an important quantum chemistry method in later years. Nowedays a DFT is main workhouse of most of the material research.

2.1.3 The Hohenberg - Kohn theorems update

The Existence Theorem

The Hohenberg-Kohn Existence Theorem establishes that the energy of a quantum system is a functional of the electron density. According to equation 2.1, the integration of the density gives us the number of electrons, so it remains to demonstrate the determination of the external potential. The theorem states that the ground-state electron density is uniquely determined by the external potential. This can be proven via *reductio ad absurdum*. [14]

The Variational Theorem

The first theorem does not provide any information how to predict the electron density of the system. In the second theorem Hohenberg and Kohn show, using the molecular orbital (MO) theory, that electron density follows the variational principle. [14]

In general if we have more *candidates* as the electron density functions, the one, that provides the lowest energy is the closest to the *true* ground state electron density (i.g. variational principle). But the theory does not provide any information on how to update the electron density function to obtain better ground state energy besides random guessing.

2.1.4 Kohn - Sham Approach

A significant inaccuracies are in the DFT calculation results from the kinetic energy approximation. Kohn - Sham idea was based on improved expression for the kinetic energy. Their approach can be described as *almost exact*. It means that the kinetic energy for the non-interacting electrons is exact. The theory uses the concept of molecular orbitals with occupancy number strictly 0 or 1. [15]

2.1.5 Local Density Approximation

The Local Density Approximation (LDA) represents any DFT functional where the value of *energy density* $\varepsilon_{\mathrm{XC}}$ at some coordinates $\boldsymbol{r}$ is computable from the value of electron density ρ in that position - from the *local position* In general only requirements for $\rho(\boldsymbol{r})$ function is that the function is unequivocal and valued at every position and it does not meter how ill-behaved the function is - the ill-behavior described in chapter 2.1.1 (e.g. cusps). However, the functionals which fit to LDA's definition are only those that are based on uniform electron gas, where the electron density is same valued in every position by its definition.

For the systems where the spin polarization is included *local spin density approximation* (LSDA) have to be used.

2.1.6 Density Gradient Approximation

In molecules and materials the electron density is typically more complex than uniform electron gas model, so the LDA approach is usually not very accurate. The way how it can be improved is that the $\varepsilon_{\mathrm{XC}}$ is dependent not only on the electron density at given point, but also on the electron density change function (i.e., its gradient). Generally, the most of the functionals are constructed with addition of correlation to the LDA functionals, e.g.:

$$\varepsilon_{\mathrm{X/C}}^{\mathrm{GGA}}(\rho(\boldsymbol{r})) = \varepsilon_{\mathrm{X/C}}^{\mathrm{LDA}} + \Delta\varepsilon_{\mathrm{X/C}}\left[\frac{|\nabla\rho(\boldsymbol{r})|}{(\rho(\boldsymbol{r}))^{\frac{4}{3}}}\right] \tag{2.9}$$

where the $\nabla\rho(\boldsymbol{r})$ term is gradient of the electron density ρ. The last term in equation 2.9 (describing the density gradient) is dimensionless quantity, not the absolute gradient of electron density function. According to mathematical definition and the fact that the first derivate of a function is also the function's property, it is more common expression for describing the dependency of the electron density and its gradient as *gradient corrected*. Upon inclusion the gradient correction into the LDA model defines the *generalized gradient approximation* (GCA).

The commonly used functionals are B88, P86 and PW91, which were described by Becke, Perdew and (Perdew and) Wang. Also the functional with no dependency on empirical parameters is PBE, described by Perdew, Burke and Ernzerhof, which has been developed by rational function expansion of the reduced gradient.

PBE functional

The method published in 1996 by John P. Perdew, Kieron Burke and Matthias Ernzerhof described improvements of Perdew-Wang 1991 (PW91) model.This is a straightforward derivation of a basic GGA method, wherein all parameters are fundamental constants. Only the fundamental aspects of the specific construction that underpins the PW91 method are utilized. Enhancements over PW91 encompass a precise depiction of the linear response of the homogeneous electron gas, appropriate performance under uniform scaling, and a smoother potential. Despite its simplicity the PBE functional gives us comparable results as more

complicated functionals from its era (e.g. PW91) and it remains commonly used functional today. [16]

2.1.7 Empirical Dispersion

The LDA and GGA functionals, including hybrid functionals, do not adequately describe the dispersion interactions in a system. Therefore, other functionals that include dispersion interaction correlation have to be utilized (e.g., non-local functionals). Another option is to include the dispersion correction to the semi-local (LDA,GGA and etc.) functionals trough empirical correction. The total energy is given by sum of usual self-consistent Kohn-Sham energy $E_{\text{KS-DFT}}$ and empirical dispersion energy E_{disp}.

$$E_{\text{DFT-D}} = E_{\text{KS-DFT}} + E_{\text{disp}} \tag{2.10}$$

In the equation 2.10 the empirical dispersion correction energy is defined by:

$$E_{\text{disp}} = -s_6 \sum_{i=1}^{N-1} \sum_{j=i+1}^{N} \frac{C_6^{ij}}{R_6^{ij}} f_{\text{dmp}}(R_{ij}) \tag{2.11}$$

where N is the number of atoms in the system, C_6^{ij} is term for dispersion coeficcient for atom pair i-j, s_6 is a global scaling factor, which depends on using density functional, and R_6^{ij} is interatomic distance in the pair ij. To avoid problems for small R like as *near-singularities*, the damping function $f_{\text{dmp}}(R_{ij})$ has to be used:

$$f_{\text{dmp}}(R_{ij}) = \frac{1}{1 + \exp(-d(\frac{R_{ij}}{R_r - 1}))} \tag{2.12}$$

where R_r is the sum of atomic and van der Waals radii. [17]

2.2 Models of hexagonal boron nitride

Boron nitride is an isoelectronic system to carbon and shares similarities with its carbon equivalents. It exists in various crystallographic forms, including cubic, hexagonal, and hexagonal nanotubes. As mentioned in the Introduction section, hexagonal boron nitride (h-BN) has been recognized as a potentially promising catalyst and offers other possibilities for use due to its favorable physical and chemical properties.

2.2.1 Cluster models

For studying the behavior of h-BN the small models were built. The h-BN is an isoelectronic system to graphene so the models were based on isoelectronic models of small aromatic hydrocarbons from benzene and naphthalene to coronene and circumcoronene. The models are shown in the figures 2.1 (models S1, S2, S3) and 2.2 (models S4, S5). All models (S1 - S5) are planar.

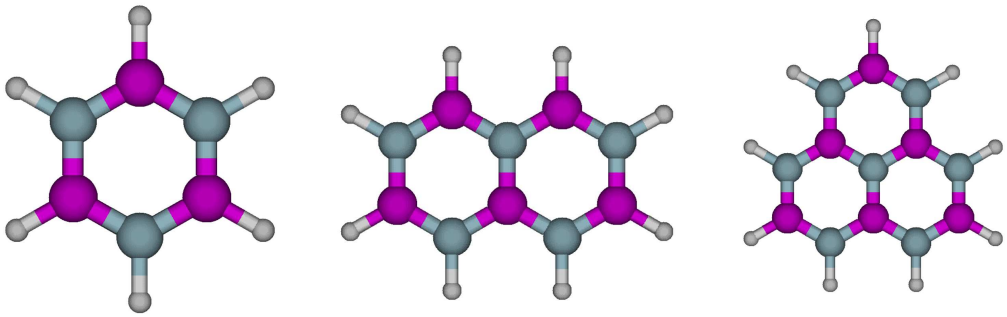

(a) S1 - *benzene like* (b) S2 - *naphthalene like* (c) S3

Figure 2.1: Small models for studying h-BN
Color legend: H - white, B - magenta, N - grey

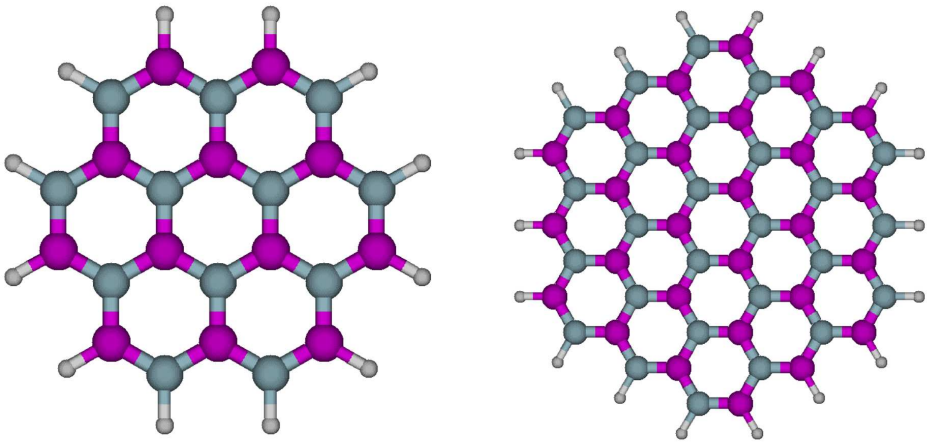

(a) S4 (b) S5

Figure 2.2: Bigger models for studying h-BN
Color legend: H - white, B - magenta, N - grey

The models depicted figures 2.1 and 2.2 are all H terminated. Based on previous research mentioned in the introduced section, the (B) - OH terminated models were prepared and studied. In the figure 2.3 is shown the comparison between (B) - OH and (B) - H terminated models.

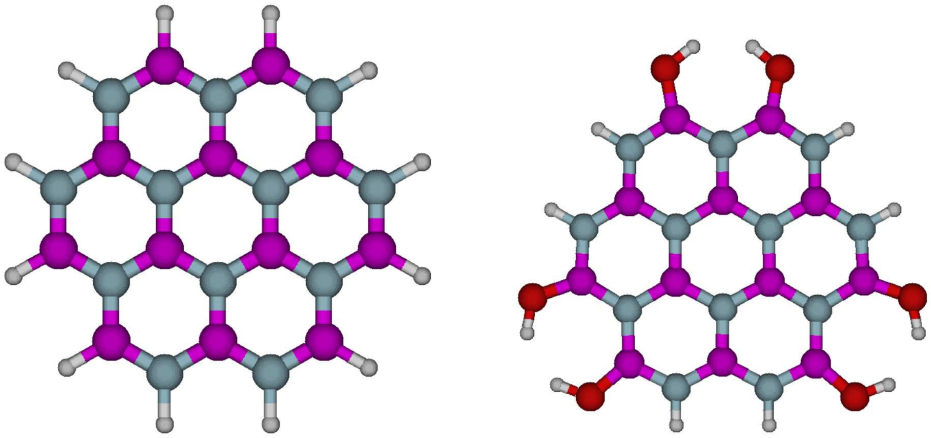

(a) S4 - H terminated boron groups (b) S4 - OH terminated boron groups

Figure 2.3: Comparison of (B)-H and (B)-OH terminated models
Color legend: H - white, B - magenta, N - grey, O - red

2.2.2 Edge models

In graphene two type of edges are commonly believed to be stable zig-zag and arm-chair types, respectively. These two types were investigated for its h-BN analogue.. The primary geometry of the edge model was generated by Matlab® script (Appendix A), so models can be prepared with substantial degree of flexibility (e.g., size, termination type). In the Figure 2.4 are shown two models that were used in this work.

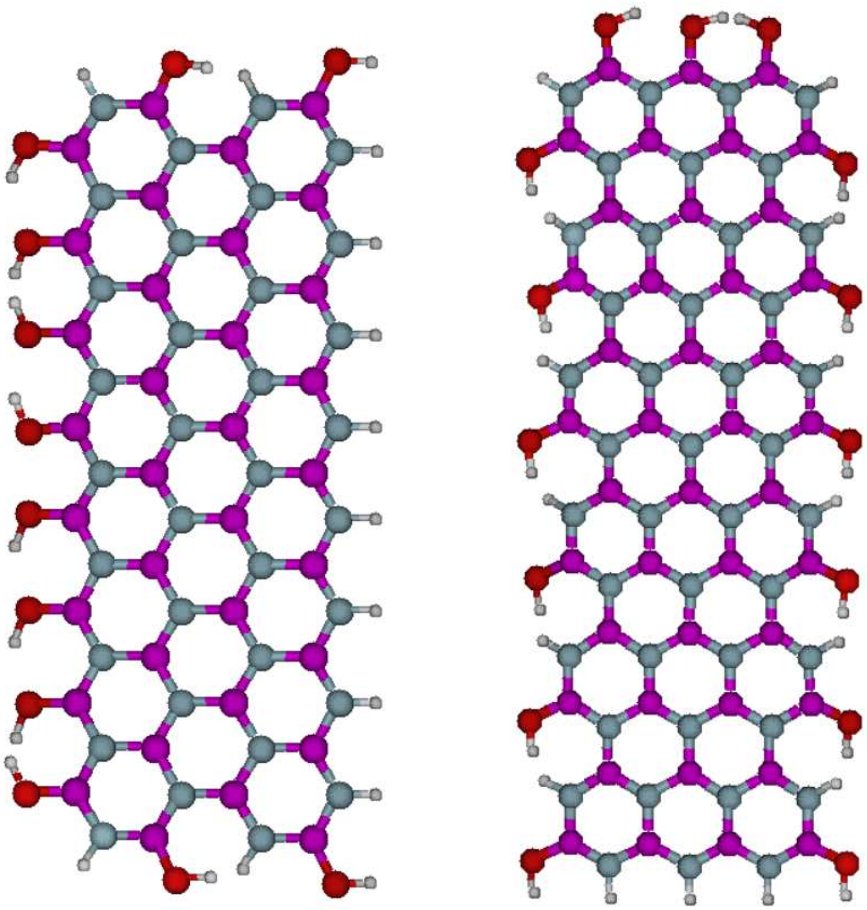

(a) *zig zag* model (b) *arm chair* model

Figure 2.4: Edge models of h-BN
Color legend: H - white, B - magenta, O - red

2.2.3 Boron oxide models

For studying interaction between boron oxides model and carbon oxide the following models in the figure 2.5 were created. The geometry of these models was suggested by Nemukhin's and Weinhold's study [18].

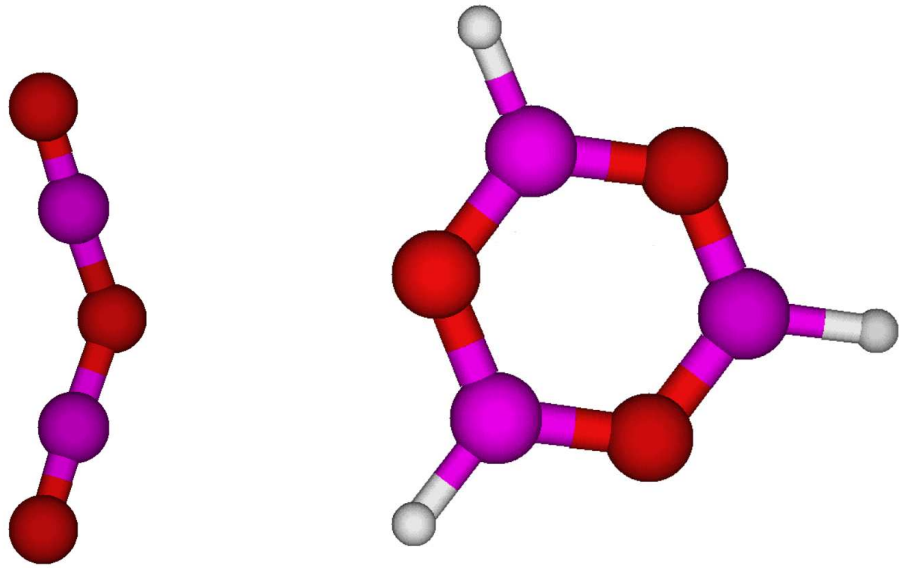

(a) B_2O_3 model (b) B_3O_3 H terminated model

Figure 2.5: Models for CO interaction with boron oxide models
Color legend: H - white, B - magenta, O - red

2.3 Computational protocol

In this section, the computational protocol used this work will be described. All calculations were performed using Gaussian 16 software [19]. The models and input files were prepared using Matlab® software, version R2022b [20] (Appendix B).

The spin-polarized calculations with PBE functional were performed using Alrich's type of basis set (def2-TZVP) [21]. The DensityFit option for all Gaussian calculations was set to speed up calculations. The density fitting is based on expanding the four-center integrals into sum of three-center integral, which yield a significant computationally time saving for medium to large model systems. The Grimme's dispersions correction model (D2) was used to account for inadequate description of dispersion interaction in PBE funcitonal.

The interaction energy between a surface(h-BN)/B_2O_3 models and radical species (O_2H, propyl radical) is defined as follows:

$$E_{\text{int}} = E(\text{surface/B2O3 + radical}) - E(\text{surface/B2O3}) - E(\text{radical}) \qquad (2.13)$$

All interaction energies are counterpoise corrected by procedure as defined by Boys and Bernardi [22]. The transition state geometries were localized using QST2 or QST3 algorithms as implemented in G16. In selected cases the harmonic frequencies were calculated to verify that local minimums were reached and analyze the positions of OH and NH bands.

3. Results

3.1 Small cluster models

3.1.1 Interaction of HOO$^{\cdot}$ specie with the H terminated models

The boron nitride ring clusters (i.e., analogues of aromatic hydrocarbons) of increasing size to model the h-BN surface were optimized at PBE-D2/def2-TZVP level of theory (see Figs. 1.1-1.3). These optimized geometries were used as an input for modeling the interaction with OOH radical due to its importance in the reactions of alkanes and O2 reaction mixtures at elevated temperatures. It is important to point out that ground state of OOH radical is doublet with a certain degree of multireference character (i.e., T1 diagnostics is about 0.03 [23]), however, it was observed that DFT methods are able to describe the multireference character of the wave functions better than standard wave functions based methods such as Hartree-Fock. The typical minimum between the h-BN surface model and OOH radical can be described as adsorption complex stabilized via dispersion interactions. Example for H - terminated S4 model is shown in the figure 3.1 (a). Another stable adsorption minimum has a covalent character (see Fig. 3.1 (b)). In case of the covalently bound OOH radical the interacting boron atom is out of plane, approx. 0.2 Å higher than other surface atoms due to the change in boron hybridization.

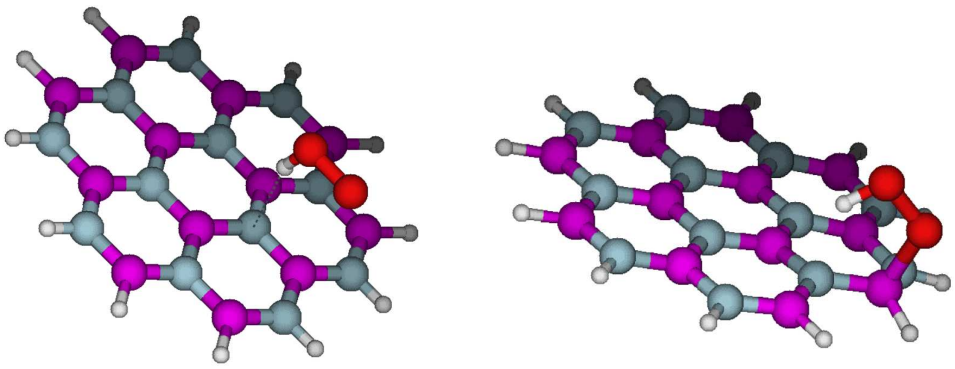

(a) Dispersion (b) Covalent

Figure 3.1: Interaction between the S4 model and OOH$^{\cdot}$ specie
Color legend: H - white, B - magenta, N - grey, O - red

Table 3.1: Differences in PBE-D2 energy between dispersal and covalent systems

Model	S1	S2	S3 *edge*	S3 *centre*	S4 *edge*
Energy difference PBE [kJ · mol^{-1}]	4.8	3.1	1.0	24.7	2.4
Energy difference PBE-D2 [kJ · mol^{-1}]	4.6	4.5	0.5	21.8	1.1

The relative stabilities of covalently bound and dispersion stabilized adsorption complexes are summarized in Table 3.1. It can be observed that the differences in the total energies of covalently bound and dispersion complexes are relatively small, only about few kJ $\cdot$ mol^{-1}. For the larger models (see Figs.2.2 and 2.3), it is possible to distinguish two types of boron atoms: (i) boron atoms that are at the cluster edge, thus needs to be terminated with hydrogen or OH group, and (ii) boron atoms that are within the cluster with neighborhood comparable to ideal h-BN surface. Significant differences are observed in relative stabilities of dispersion and covalently bound complexes upon OOH adsorption on these two types of boron atoms. The edges exhibit a very low energy differences between the dispersion stabilized and covalently bound adsorption complexes, respectively. In contrasts, this energy difference significantly increases for OOH adsorption on boron within the cluster. Furthermore for S4 models (i.e., analogues of coronene), the stable minimum on potential energy surface for covalently bound complex with OOH was not found. This observation strongly supports that the experimentally observed B_2O_3 particles are formed on the edges/defects of the h-BN structure. Generally, there were no significant differences in the results obtained with or without the empirical dispersion correction.

Table 3.2: PBE-D2 interaction energy between small models and OOH$^{\bullet}$ specie

Model	S1	S2	S3	S4
Interaction energy [kJ $\cdot$ mol^{-1}]	31.9	29.8	32.4	30.0

Table 3.3: Boron - Oxygen distance in dispersal and covalent system of S3 model and OOH$^{\bullet}$ specie. PBE-D2 theory level

	Covalent	Transit state	Dispersal
Distance B-O [Å]	1.7062	2.0261	2.7854
Distance N-H [Å]	1.8441	1.8902	2.0751

The interaction energy was also evaluated, and no significant differences were found between the models (S1-S4), the results are shown in Table 3.2. For all models, the PBE-D2 interaction energy, between the H-terminated models of h-BN surface and the HOO radical, is approximately 30 kJ $\cdot$ mol^{-1}. Although, the relative energy differences between the dispersion and covalently bound complexes are small, there is question, whether there is a larger barrier in the formation of covalently bound complex. The located transition state for S3 model is shown in Figure 3.2 and geometry parameters are summarized in Table 3.3. The barrier is quite negligible (5 kJ $\cdot$ mol^{-1}) due to fact that only energy penalty seems to be weaking of the hydrogen bond and electronic effects are of substantial lesser importance.

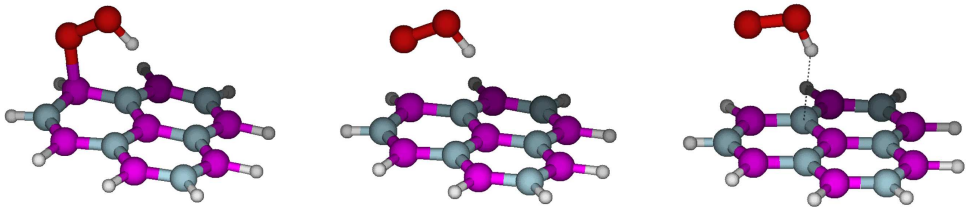

(a) Covalent (b) Transit state (c) Dispersal

Figure 3.2: Transition state between covalent and dispersal state of the S3 model and $OOH^{\bullet}$ specie
Color legend: H - white, B - magenta, N - grey, O - red

3.1.2 Interaction of $HOO^{\bullet}$ specie with the OH terminated models

In OH-terminated models, a formation of of the double hydrogen bond interactions is observed. Figure 3.3 depicts such an interaction in the S2OH model. In this case, the interaction energy is nearly double, with a value of 57.3 $kJ \cdot mol^{-1}$ compared to 29.8 $kJ \cdot mol^{-1}$ in the H-terminated model. Moreover, the increased interaction is also reflected in shortening of the hydrobon bond distance from 2.07 Å to 1.91 Å.

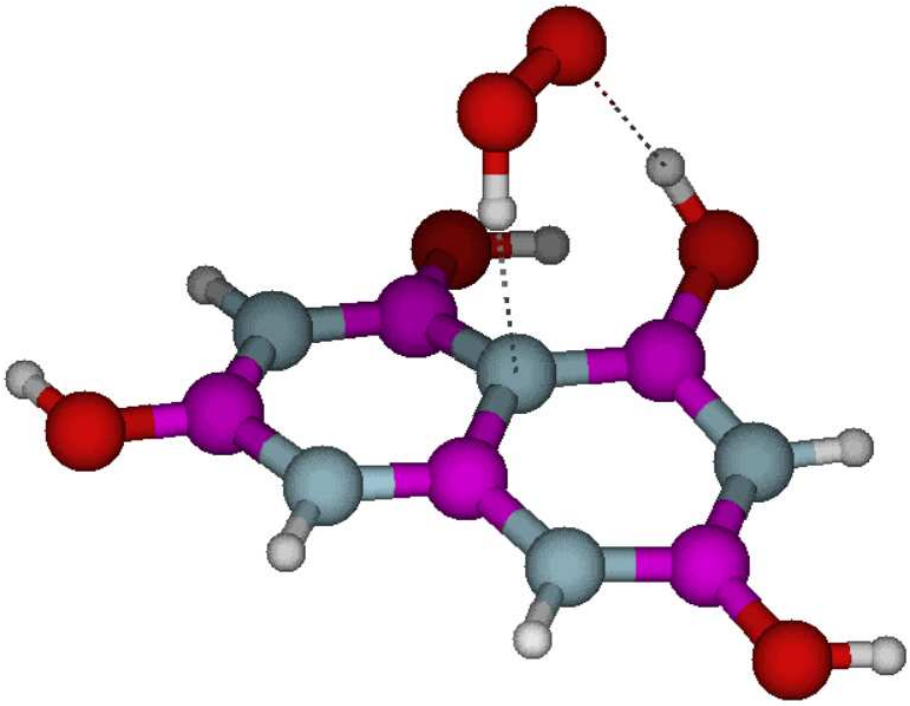

Figure 3.3: Double hydrogen bond in S2OH model
Color legend: H - white, B - magenta, N - grey, O - red

The energy differences between the covalently bound and dispersion complexes with one hydrogen bond are independent on the model termination.
Clearly the adsorption complexes stabilized by two hydrogen bonds, as in the Figure 3.3, the energy difference is increased from approx. 1 - 4 kJ $\cdot$ mol^{-1}to approx. 25 kJ $\cdot$ mol^{-1}. This stabilization is also reflected in the corresponding barrier of the transitions state.

3.1.3 Interaction of propyl radical with models

The interaction of h-BN model surface with two possible propyl radicals, primary and secondary, was investigated (see Figure 3.4). The calculated interaction energies are summarized in Table 3.4. The propyl radical interacts with the h-BN surface model mainly via dispersion stabilization and the formation of covalent interaction between the propyl radical and the surface was not observed.

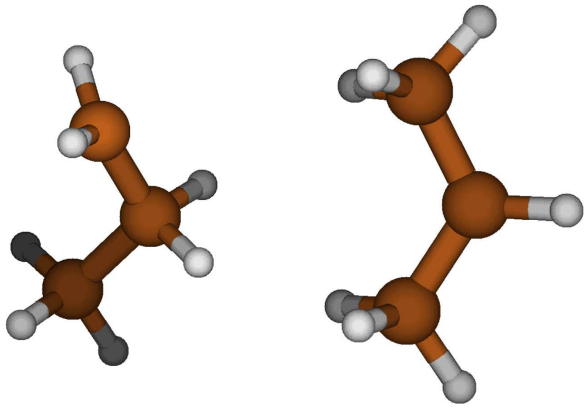

(a) Primary (b) Secondary

Figure 3.4: Propyl radicals
Color legend: H - white, C - brown

Generally, the H terminated models have lower interaction energies upon comparison with OH terminated models. However, this difference decreasing with the model size, indicating that edges may be slightly preferable adsorption sites for the propyl radical. The difference in interaction energies of primary and secondary propyl radical seems to be insignificant and general trend was not found.

3.2 Edge models

The the optimized structures of the edge models are shown in Figure 3.5 for the *arm-chair* model and Figure 3.6 for the *zig-zag* structure. The located stable minimum structures (confirmed via harmonic frequency analysis) are deformed at the edges (i.e., BN atoms are out of plane from the rest of the h-BN surface).

Table 3.4: PBE-D2 interaction energies between models and propyl radical

Model	**Reactant**	**Interacting energy** [kJ · mol^{-1}]
S1	1	17,2
S2	1	23,1
S3	1	23,0
S4	1	30,0
S1OH	1	19,2
S2OH	1	24,4
S3OH	1	35,9
S4OH	1	31,6
S1	2	16,5
S2	2	21,1
S3	2	25,7
S4	2	30,5
S1OH	2	28,2
S2OH	2	22,5
S3OH	2	29,5
S4OH	2	32,1

Legend: Reactant 1 - primary propyl radical, Reactant 2 - secondary propyl radical

The *zig-zag* model has 3 positions for OH terminating groups, as shown in Figure 3.6. In the first case (a) the hydrogen of the OH group has the same orientation as the hydrogen in the next OH group, and both OH groups are in the same half-space (plane is defined by the model's surface). In second case (b) the two hydrogens of the adjacent OH groups are opposite each other and are oriented towards different half-spaces. The results of case (a) and (b) are combined in case (c), where the hydrogens are oriented in opposite directions out from the second hydrogen, also in different half-spaces.

3.2.1 Reactivity with $OOH^{\cdot}$ specie

Although with cluster models the covalently bound adsorption complex was observed (see Chapter 3.1.1)), for all investigated edge models only the dispersion stabilized adsorption complexes were found, which would indicate a lower reactivity of the zig-zag and arm-chair edges with respect to previously investigated cluster models. Furthermore, the fact that the covalently bound OOH radical is not observed at the zig-zag and arm-chair edges may suggest that the initial steps of the ODH process are not located on them.

The interaction energies between the OOH radical and the edge surface models depend on the position of the OOH species above the surface, ranging from 37 to 60 kJ · mol^{-1}. These values align closely with the interaction energies calculated for small cluster models discussed in Chapter 3.1.1. The dependency lies in the location of the OOH species, specifically whether the OOH radical can interact with the surface through more than one hydrogen bond.

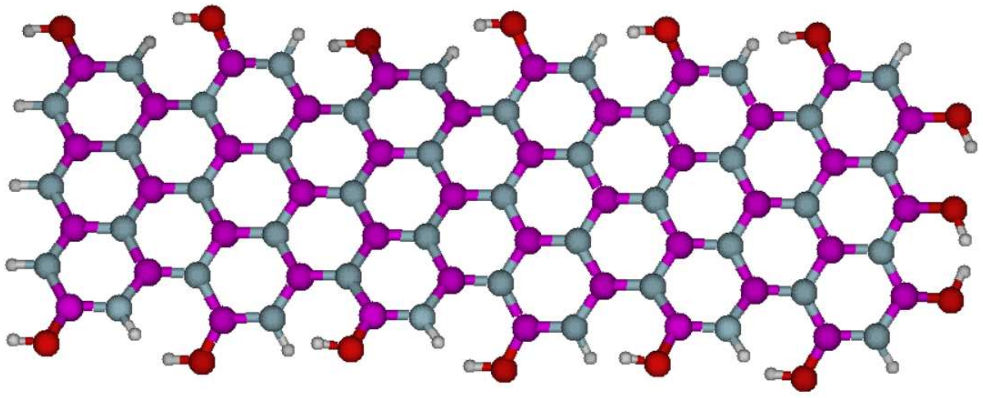

(a) Top view

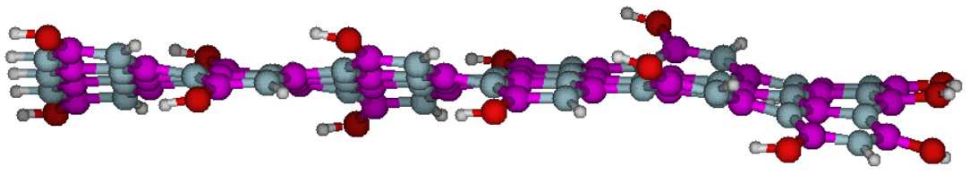

(b) Side view

Figure 3.5: *Arm chair* edge model optimized geometry
Color legend: H - white, B - magenta, N - grey, O - red

3.2.2 Reactivity with propyl radical

In the Table 3.5 the interaction energies of propyl radical with the h-BN edge surface models are summarized. The interaction energies closely resemble the values calculated for small cluster models (cf. Table S4). In can be concluded, that arm-chair and zig-zag edges do not form covalently bound complexes with propyl radical, but interact only via dispersion interactions. Thus, it rules out the ODH mechanism, where propyl radicals are "*captured*" by edges on the h-BN surface.

Table 3.5: PBE-D2 interaction energy of propyl radical and edge surface models

Model	**Reactant**	**Interacting energy** [kJ $\cdot$ mol^{-1}]
zig zag	1	30,6
arm chair	1	32.6
zig zag	2	34,2
arm chair	2	35,9

Legend: Reactant 1 - primary propyl radical, Reactant 2 - secondary propyl radical

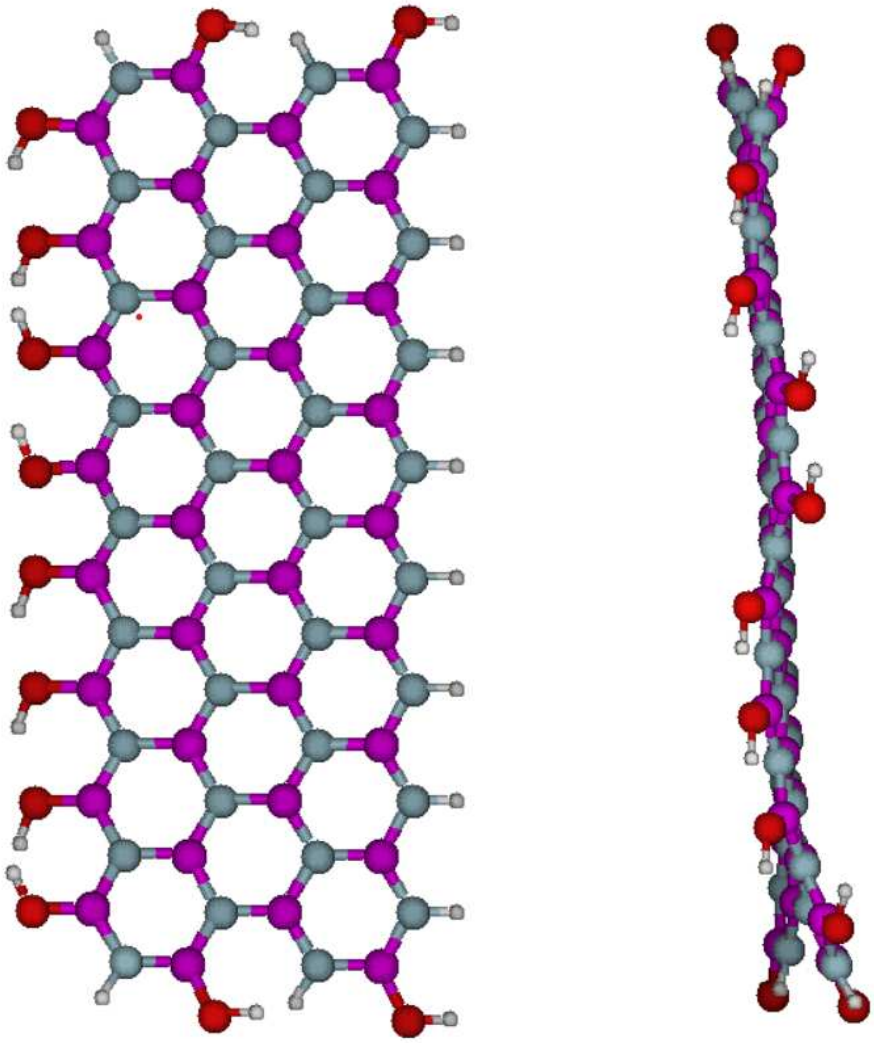

(a) Top view (b) Side view

Figure 3.6: *Zig zag* edge model optimized geometry
Color legend: H - white, B - magenta, N - grey, O - red

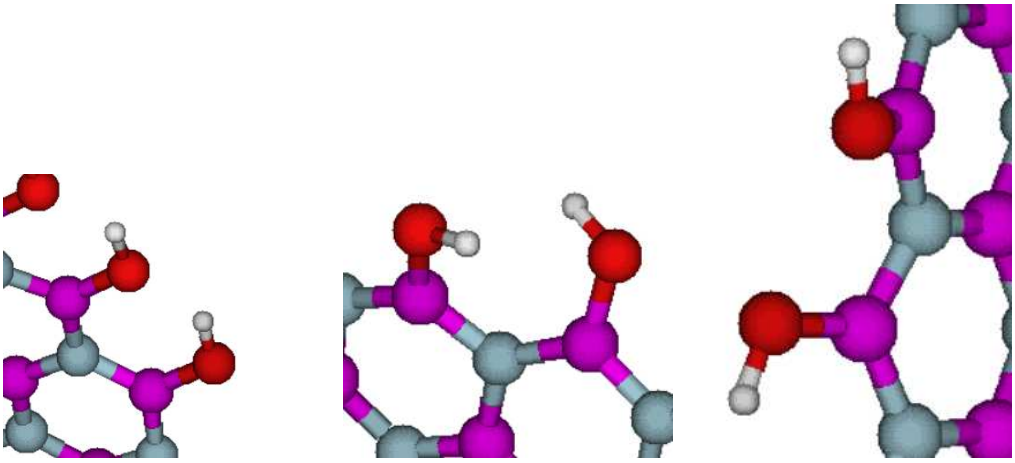

(a) (b) (c)

Figure 3.7: Orientation of OH group in *Zig zag* edge model
Color legend: H - white, B - magenta, N - grey, O - red

3.2.3 Frequency analysis

The edge model include (B)-O-H terminated groups, which frequencies were analyzed to compare them against experimentally measured infrared spectra. According to beginning of section 3.2, there are three possible orientations of OH groups at the edge: one *arm chair* and two *zig zag* orientations[1]. Besides OH groups, the edge model also includes N-H terminated groups. The frequency analysis was provided for separate edge model and also for systems where the edge models interacted with OOH radical.

N-H frequency

In the *arm chair* edge model N-H frequency is 3500 cm^{-1} and in the *zig zag* edge model 3520 cm^{-1} . These N-H groups are shown in the Figure 3.8. There is no observable changes in the N-H frequency upon interaction with OOH and propyl radicals.

O-H frequency

In the *zig zag* edge model, two distinct frequency bands corresponding to OH vibrations are observed. The first frequency band, ranging from 3570 to 3586 cm^{-1} , arises from OH groups with the same orientation (Figure 3.7(a)). The second frequency band results from neighboring OH groups with opposite orientations (Figure 3.7(b)), exhibiting frequencies between 3690 and 3710 cm^{-1} . On the other hand, the OH frequency band in the *arm chair* edge model is observed in the range of 3665 to 3685 cm^{-1} .

Comparing the OH group frequencies to NH groups, noticeable differences can be observed. In the system involving the (primary) propyl radical, the OH group frequency at the *zig zag* edge model, specifically pointing to the propyl

[1]The (c) case presented in Figure 3.7 is a consequence of the presence of both (a) and (b) possibilities in the edge, and thus these sites were not investigated.

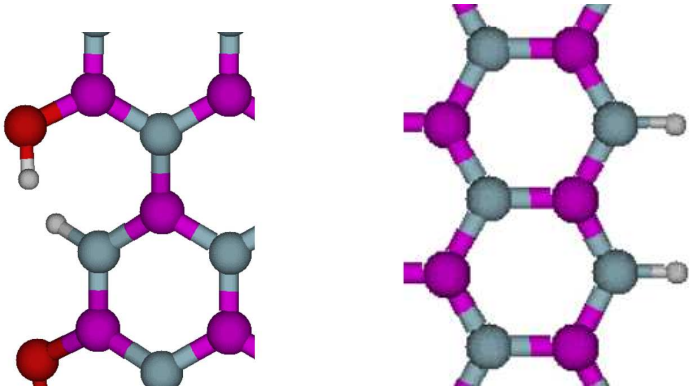

(a) In *armchair* (b) In *zig zag*

Figure 3.8: N-H groups in edge models
Color legend: H - white, B - magenta, N - grey, O - red

radical (Figure 3.9), is red-shifted to 3332 cm^{-1} . Additionally, when interacting with an OOH radical (Figure 3.10), the frequency of the nearest[2] OH group at the edge of the surface changes to 3417 cm^{-1} . The comparison with experimental values cannot be performed on absolute values of calculated frequencies, but upon scaling the calculated bands fit quite well in the experimentally measured spectrum. However, the experimental resolution is not sufficient to unambiguously assign the vibrational bands, thus back-to-back comparison with calculated values is problematic.

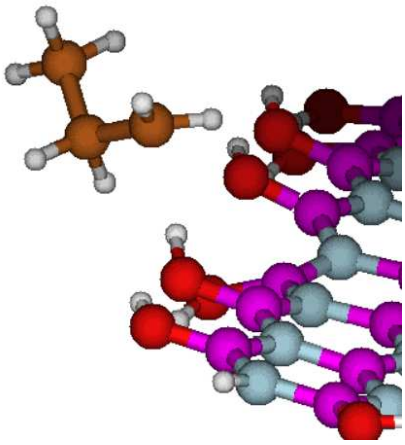

Figure 3.9: Interacting propyl radical

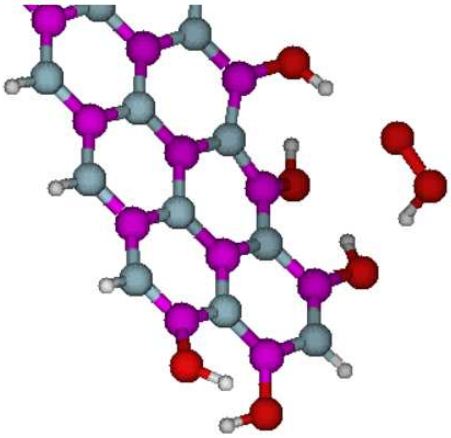

Figure 3.10: Interacting $OOH^{\bullet}$ specie

Color legend: H - white, B - magenta, C - brown, N - grey, O - red

3.3 Boron oxide models

The investigation focused on small clusters of boron oxide as models of a 'spent' catalyst. The primary objective was to determine if it is possible to characterize

[2]The OH edge group with changed frequency is that one, which is close to H atom in OOH specie . The OH group near oxygen atom of OOH specie has same frequency as without interaction with OOH specie.

active sites within the catalyst by studying the adsorption of probe molecules. Carbon monoxide (CO) was chosen as the probe molecule due to its distinctive vibrational frequency, which is highly sensitive to the specific interaction between CO and the material (e.g., acid sites in molecular sieves).

The boron oxide geometries proposed in the literature were optimized at DFT level of theory, and these optimized geometries were used as inputs for subsequent analyses. This chapter explores the interaction between these boron oxide models and carbon monoxide (CO). Most of the resulting complexes were stabilized via dispersion interactions, regardless of the orientation of the CO molecule relative to the boron oxide model (see Figures 3.11(a), 3.11(b), and 3.12). However, in one particular case illustrated in Figure 3.11(c), a covalent interaction was observed between the B_2O_3 model and the CO molecule when it was oriented with its carbon atom facing the boron oxide model. Thus, it indicates that CO can specifically interact with unsaturated boron sites of the h-BN catalyst.

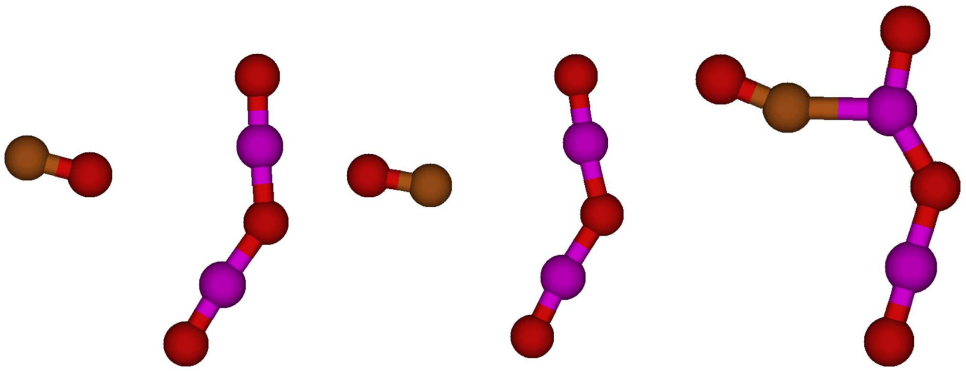

(a) (b) (c)

Figure 3.11: B_2O_3 interaction with carbon oxide
Color legend: B - magenta, C - brown, O - red

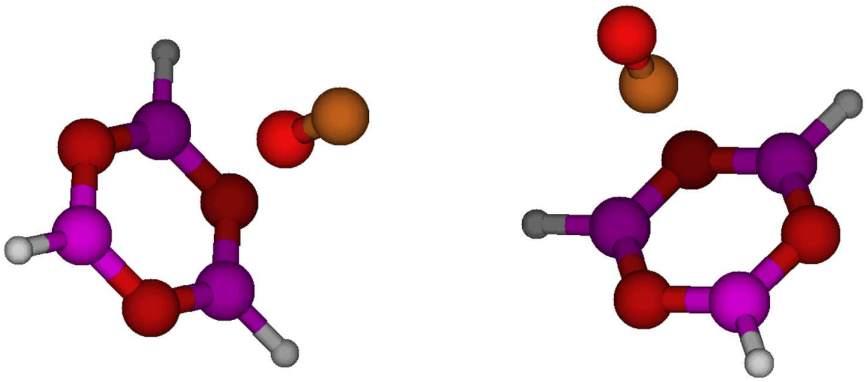

(a) (b)

Figure 3.12: B_3O_3 interaction with carbon oxide
Color legend: H - white, B - magenta, C - brown, O - red

3.3.1 Frequency analysis

In the models shown in the Figures 3.11 and 3.12. The shift in CO frequency was determined by calculating the difference between the CO frequency in the gas phase and the CO frequency in the system with a boron oxide model.

$$\Delta\nu(\mathrm{CO}) = \nu(\mathrm{CO}) - \nu(\mathrm{CO;\ boron\ oxide\ model}) \tag{3.1}$$

Generally, the sign of frequency shift $\Delta\nu$ is positive ($\Delta\nu > 0$) when the carbon oxide is oriented to boron oxide model with its oxygen models, and negative in opposite cases - when the carbon oxide is oriented to boron oxide with its carbon atom.

All results are shown in the Table 3.6. The lowest frequency shift is observed for model with covalent interaction (B_2O_3 (c)). For the B_2O_3 models the higher shifts in frequency are obtained, comparing to B_3O_3 models (excluding covalent bonding system). This observation was confirmed experimentally, where all frequency shifts were quite small, thus usually indicating only dispersion stabilized adsorption complexes of the CO on the surface. Surprisingly even the case of covalently bound CO exhibits only minimal shift in CO frequency.

Table 3.6: Results for boron oxide models on PBE-D2 theory level

Model	**ID**	$\Delta\nu$(CO) [cm^{-1}]	E_{int} [kJ $\cdot$ mol^{-1}]
B_2O_3	(a)	$+11,2$	8,5
B_2O_3	(b)	$-22,9$	19
B_2O_3	(c)	$-2,68$	92
B_3O_3	(a)	$+5,76$	5,7
B_3O_3	(b)	$-8,96$	7,9

$\Delta\nu$(CO) is a frequency shift of carbon oxide; E_{int} is interaction energy
Legend according the Figures 3.11 and 3.12

3.3.2 Interaction energy analysis

The calculation of interaction energies for these models, as presented in Table 3.6, reveals that the boron oxide and carbon oxide models exhibit higher interaction energies when the oxygen atom of CO is in closer proximity to the boron oxide species, compared to situations where the CO interacts via C-end. The notable exception is the carbon oxide bonded to the boron oxide model through a B-C bond, which exhibits the highest interaction energy of 92 kJ $\cdot$ mol^{-1}. Additionally, the B_2O_3 models show greater differences in interaction energies based on the orientation of carbon oxide, compared to the B_3O_3 models. This points towards the conclusion that in order to locate these unsaturated boron adsorption sites the calorimetry measurements might provide a better insight into the 'spent' catalyst behavior than FT-IR measurments.

Conclusion

This thesis investigates the preliminary research on the initial steps of the ODH process of alkanes. Small to medium-sized cluster models of h-BN surfaces were constructed, with a primary focus on the interaction of these models with radicals. These radicals are formed when propane and O_2 are mixed at elevated temperatures and are believed to be responsible for the initial steps of the ODH process on this type of surface.

Two types of complexes with the OOH radical were observed: dispersion-stabilized complexes and covalently bound complexes. The covalently bound complexes tend to form on the edge boron atoms. Interestingly, the *zig zag* and *arm chair* edges do not form stable covalently bound complexes with OOH radicals. In contrast, the edge B-OH groups can form a hydrogen bond with OOH species, which can be further stabilized with a second hydrogen bond to the nitrogen of the h-BN surface model, resulting in an interaction energy of $60 \ \text{kJ} \cdot \text{mol}^{-1}$.

The propyl radicals, whether primary or secondary, do not form covalently bound complexes with the h-BN surface models, suggesting that the surface does not seem to "capture" propyl radicals, ruling out one of the mechanisms proposed in the literature. Analysis of the O-H and N-H frequencies revealed significantly shifted OH bands on different edges. However, the spectra obtained experimentally do not have sufficient resolution to unambiguously assign these bands.

It has been established that B_2O_3 particles are formed on the h-BN surface. Simple models of B2O3 species were explored as a model of a spent catalyst, and their interaction with carbon monoxide (CO) as a probe was addressed. While CO can strongly interact with unsaturated boron atoms, no shift in CO frequency was observed. In contrast, calorimetry measurements of CO on activated h-BN surfaces can indicate catalytically active sites.

Bibliography

[1] Jian Sheng, Bing Yan, Wen-Duo Lu, Bin Qiu, Xin-Qian Gao, Dongqi Wang, and An-Hui Lu. Oxidative dehydrogenation of light alkanes to olefins on metal-free catalysts. *Chem. Soc. Rev.*, 50:1438–1468, 2021.

[2] O.V Buyevskaya and M Baerns. Catalytic selective oxidation of propane. *Catalysis Today*, 42(3):315–323, 1998.

[3] Jinshu Tian, Jiwei Li, Shuya Qian, Zhaoxia Zhang, Shaolong Wan, Shuai Wang, Jingdong Lin, and Yong Wang. Understanding the origin of selective oxidative dehydrogenation of propane on boron-based catalysts. *Applied Catalysis A: General*, 623:118271, 2021.

[4] M.M Bhasin, J.H McCain, B.V Vora, T Imai, and P.R Pujadó. Dehydrogenation and oxydehydrogenation of paraffins to olefins. *Applied Catalysis A: General*, 221(1):397–419, 2001. Hoelderich Special Issue.

[5] Wei Qi and Dangsheng Su. Metal-free carbon catalysts for oxidative dehydrogenation reactions. *ACS Catalysis*, 4(9):3212–3218, Sep 2014.

[6] J. T. Grant, C. A. Carrero, F. Goeltl, J. Venegas, P. Mueller, S. P. Burt, S. E. Specht, W. P. McDermott, A. Chieregato, and I. Hermans. Selective oxidative dehydrogenation of propane to propene using boron nitride catalysts. *Science*, 354(6319):1570–1573, 2016.

[7] John H. Knox. The gaseous products from the oxidation of propane at 318°c. *Trans. Faraday Soc.*, 56:1225–1234, 1960.

[8] Zihao Zhang, Jinshu Tian, Xiangkun Wu, Ivan Surin, Javier Pérez-Ramírez, Patrick Hemberger, and Andras Bodi. Unraveling radical and oxygenate routes in the oxidative dehydrogenation of propane over boron nitride. *Journal of the American Chemical Society*, 145(14):7910–7917, Apr 2023.

[9] Hongping Li, Jinrui Zhang, Peiwen Wu, Suhang Xun, Wei Jiang, Ming Zhang, Wenshuai Zhu, and Huaming Li. O2 activation and oxidative dehydrogenation of propane on hexagonal boron nitride: Mechanism revisited. *The Journal of Physical Chemistry C*, 123(4):2256–2266, Jan 2019.

[10] Rui Huang, Bingsen Zhang, Jia Wang, Kuang-Hsu Wu, Wen Shi, Yajie Zhang, Yuefeng Liu, Anmin Zheng, Robert Schlögl, and Dang Sheng Su. Direct insight into ethane oxidative dehydrogenation over boron nitrides. *ChemCatChem*, 9(17):3293–3297, 2017.

[11] Lei Shi, Bing Yan, Dan Shao, Fan Jiang, Dongqi Wang, and An-Hui Lu. Selective oxidative dehydrogenation of ethane to ethylene over a hydroxylated boron nitride catalyst. *Chinese Journal of Catalysis*, 38(2):389–395, 2017.

[12] Mehdi D. Esrafili and Roghaye Nurazar. A dft study on the possibility of using boron nitride nanotubes as a dehydrogenation catalyst for methanol. *Applied Surface Science*, 314:90–96, 2014.

[13] C.J. Cramer. *Essentials of Computational Chemistry: Theories and Models*. Wiley, 2005.

[14] P. Hohenberg and W. Kohn. Inhomogeneous electron gas. *Phys. Rev.*, 136:B864–B871, Nov 1964.

[15] W. Kohn and L. J. Sham. Self-consistent equations including exchange and correlation effects. *Phys. Rev.*, 140:A1133–A1138, Nov 1965.

[16] John P. Perdew, Kieron Burke, and Matthias Ernzerhof. Generalized gradient approximation made simple. *Phys. Rev. Lett.*, 77:3865–3868, Oct 1996.

[17] Stefan Grimme. Semiempirical gga-type density functional constructed with a long-range dispersion correction. *Journal of Computational Chemistry*, 27(15):1787–1799, 2006.

[18] A. V. Nemukhin and F. Weinhold. Boron oxides: Ab initio studies with natural bond orbital analysis. *The Journal of Chemical Physics*, 98(2):1329–1335, 01 1993.

[19] M. J. Frisch, G. W. Trucks, H. B. Schlegel, G. E. Scuseria, M. A. Robb, J. R. Cheeseman, G. Scalmani, V. Barone, G. A. Petersson, H. Nakatsuji, X. Li, M. Caricato, A. V. Marenich, J. Bloino, B. G. Janesko, R. Gomperts, B. Mennucci, H. P. Hratchian, J. V. Ortiz, A. F. Izmaylov, J. L. Sonnenberg, D. Williams-Young, F. Ding, F. Lipparini, F. Egidi, J. Goings, B. Peng, A. Petrone, T. Henderson, D. Ranasinghe, V. G. Zakrzewski, J. Gao, N. Rega, G. Zheng, W. Liang, M. Hada, M. Ehara, K. Toyota, R. Fukuda, J. Hasegawa, M. Ishida, T. Nakajima, Y. Honda, O. Kitao, H. Nakai, T. Vreven, K. Throssell, J. A. Montgomery, Jr., J. E. Peralta, F. Ogliaro, M. J. Bearpark, J. J. Heyd, E. N. Brothers, K. N. Kudin, V. N. Staroverov, T. A. Keith, R. Kobayashi, J. Normand, K. Raghavachari, A. P. Rendell, J. C. Burant, S. S. Iyengar, J. Tomasi, M. Cossi, J. M. Millam, M. Klene, C. Adamo, R. Cammi, J. W. Ochterski, R. L. Martin, K. Morokuma, O. Farkas, J. B. Foresman, and D. J. Fox. Gaussian˜16 Revision C.01, 2016. Gaussian Inc. Wallingford CT.

[20] The MathWorks Inc. Matlab version: 9.13.0 (r2022b), 2022.

[21] Florian Weigend. Accurate coulomb-fitting basis sets for h to rn. *Physical Chemistry Chemical Physics*, 8(9):1057–1065, 2006.

[22] S.F. Boys and F. Bernardi. The calculation of small molecular interactions by the differences of separate total energies. some procedures with reduced errors. *Molecular Physics*, 19(4):553–566, 1970.

[23] Jiří Čížek. *On the Use of the Cluster Expansion and the Technique of Diagrams in Calculations of Correlation Effects in Atoms and Molecules*, pages 35–89. John Wiley and Sons, Ltd, 1969.

List of Figures

List of Tables

List of Abbreviations

BNNT	boron nitride nanotubes
DFT	density functional theory
DH	dehydrogenation process
h-BN	hexagonial boron nitride
ODH	Oxidative Dehydrogenation process

Appendix A

MATLAB *arm chair* edge surface model code

```
clc
clear
close all

cd ..
cd ..
numplusrings = 7;
numrings = 2;
T = table();

T.Atom = ["B"];
T.x = 0.01;
T.y = 0.01;
T.z = 0.01;



T = pridejatom("N",T,1,12);
T = pridejatom("B",T,2,1);
T = pridejatom("N",T,3,4);
T = pridejatom("B",T,4,6);
T = pridejatom("N",T,5,7);

for i = 1:numrings
   T = pridejatom("B",T,4*i,1);
   lam = height(T);
   T = pridejatom("N",T,lam,4);
   T = pridejatom("B",T,lam+1,6);
   T = pridejatom("N",T,lam+2,7);
end


i = 1;
```

```
T = pridejatom("N",T,4*i-1,12);

vzd = T.x(end) - T.x(6);
T(end,:) = [];

newT = T;
for j = 1:numplusrings
```

```
    newNewT = newT;
    newNewT.x = newNewT.x + (j*vzd);
    T = [T; newNewT];
end

ID = find(T.x == min(T.x) & T.Atom == "N");
for i = 1:length(ID)
    T = pridejatom("H",T,ID(i),6);
end
ID = find(T.x == max(T.x) & T.Atom == "B");
for i = 1:length(ID)
    T = pridejatom("O",T,ID(i),12);
   lam = height(T);
   T = pridejatom("H",T,lam,12);
end

ID = find(T.y == min(T.y) & T.Atom == "B");
for i = 1:length(ID)
    T = pridejatom("O",T,ID(i),9);
   lam = height(T);
   T = pridejatom("H",T,lam,9);
end
ID = find(T.y == max(T.y) & T.Atom == "B");
for i = 1:length(ID)
    T = pridejatom("O",T,ID(i),3);
   lam = height(T);
   T = pridejatom("H",T,lam,3);
end
ID = find(abs(T.y - min(T.y)) < 2.5 & T.Atom == "N");
for i = 1:length(ID)
    T = pridejatom("H",T,ID(i),9);
end
ID = find(abs(T.y - max(T.y)) < 2.5 & T.Atom == "N");
for i = 1:length(ID)
    T = pridejatom("H",T,ID(i),3);
end
figure()
hold on

plotT = T(T.Atom == "B",:)
```

	Atom	x	y	z
1	"B"	0.0100	0.0100	0.0100
2	"B"	1.9600	1.1358	0.0100
3	"B"	0.0100	2.2617	0.0100
4	"B"	1.9600	3.3875	0.0100
5	"B"	0.0100	4.5133	0.0100
6	"B"	1.9600	5.6392	0.0100
7	"B"	0.0100	6.7650	0.0100
8	"B"	3.9100	0.0100	0.0100
9	"B"	5.8600	1.1358	0.0100
10	"B"	3.9100	2.2617	0.0100
11	"B"	5.8600	3.3875	0.0100
12	"B"	3.9100	4.5133	0.0100
13	"B"	5.8600	5.6392	0.0100
14	"B"	3.9100	6.7650	0.0100

```
plot(plotT.x,plotT.y,"redx")
plotT = T(T.Atom == "N",:);

plot(plotT.x,plotT.y,"bluex")
plotT = T(T.Atom == "H",:);

plot(plotT.x,plotT.y,"blackx")
plotT = T(T.Atom == "O",:);

plot(plotT.x,plotT.y,"blacko")
axis("equal")

cd input_files\structure11\
```

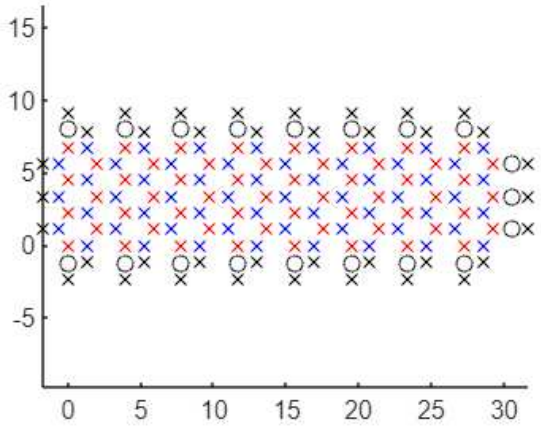

```
function novatabulka = pridejatom(atomsymbol, tabulka, ...
     odkud, pozice)
vaz_delka = 1.3;
if atomsymbol == "H"
    vaz_delka = 1.1;
end
syms x y
dX = double(solve(cosd(60) == sum([vaz_delka 0 0] .* ...
    [x y 0]) / vaz_delka^2,x));
dY = double(solve( sqrt(sum([dX^2 y^2])) == vaz_delka));
dY = abs(dY(1));
novatabulka = table();
novatabulka.Atom = atomsymbol;
novatabulka.x = tabulka.x(odkud);
novatabulka.y = tabulka.y(odkud);
novatabulka.z = tabulka.z(odkud);

switch pozice
    case 12
        novatabulka.x = novatabulka.x + vaz_delka;
    case 1
        novatabulka.x = novatabulka.x + dX;
        novatabulka.y = novatabulka.y + dY;
    case 3
        novatabulka.y = novatabulka.y + vaz_delka;
    case 4
        novatabulka.x = novatabulka.x - dX;
        novatabulka.y = novatabulka.y + dY;
    case 6
        novatabulka.x = novatabulka.x - vaz_delka;
    case 7
        novatabulka.x = novatabulka.x - dX;
        novatabulka.y = novatabulka.y - dY;
    case 9
        novatabulka.y = novatabulka.y - vaz_delka;
    case 10
        novatabulka.x = novatabulka.x + dX;
        novatabulka.y = novatabulka.y - dY;
end
novatabulka = [tabulka; novatabulka];

end
```

Appendix B

MATLAB reaction model script

```
clc
clear
close all

%user input
reakcniatom = 51
empdis = 1
reaction = 42
c = 4
save = 1
minus = 0

cd ..\..\
load OOH.mat
cd input_files\43\

cd edges\Excel\
DIR = dir("*sour*");
DIR = struct2table(DIR);
DIR.name = string(DIR.name);
cd ..\..\

name = DIR.name(c);
cd edges\Excel\

T = readtable(name);
T = zpracujtabulku(T);
cd ..\..\

tx = str2double(T.X(reakcniatom))
```

```
tx = 1.1901
```

```
ty = str2double(T.Y(reakcniatom))
```

```
ty = 1.2427
```

```
tz = str2double(T.Z(reakcniatom))
```

```
tz = 0.1946
```

```
newT = table();
newT.Atom = ["O"; "O"; "H"];
if minus == 1
    newT.X = string(-OOH(:,1) + tx);
    newT.Y = string(-OOH(:,2) + ty);
    newT.Z = string(-OOH(:,3) + tz);
else
    newT.X = string(OOH(:,1) + tx);
    newT.Y = string(OOH(:,2) + ty);
    newT.Z = string(OOH(:,3) + tz);

end

T = [T; newT];

name = extractBefore(name,"sour")
```

```
name = "s11_5_3_edge2_2"
```

```
  if save == 1
savefilename = strjoin([name "_r" string(reaction) "_" ...
    string(reakcniatom)],"");
if minus == 1
    savefilename = strrep(savefilename,"_r","_rm");
end
chkfilename = strjoin(["%%chk=" savefilename ".chk"],"")
savefilename = strjoin([savefilename ".gau"],"")

fileID2 = fopen(savefilename,'w');
fprintf(fileID2,'%%mem=20000MB\n');
fprintf(fileID2,char(chkfilename),'char');
fprintf(fileID2,'\n','char');
if empdis == 0
fprintf(fileID2,'#p PBEPBE/Def2TZVP DensityFit Opt \n\n');
else
fprintf(fileID2,'#p PBEPBE/Def2TZVP EmpiricalDispersion=GD2 ...
     DensityFit Opt \n\n');
end
fprintf(fileID2,char(strjoin(["BN_surf_OH" ...
    extractBefore(savefilename,".gau")],"_")));
fprintf(fileID2,'\n\n0 2 \n','char')


for i = 1:height(T)
    C = strjoin(table2array(T(i,:))," ");
    C = strrep(C,"0.000","0.001");
    fprintf(fileID2,C,'char');
```

```
    fprintf(fileID2,'\n','char');
end
fprintf(fileID2,'\n','char');
fclose(fileID2);


end


function T = zpracujtabulku(wT)


wT.AtomicNumber = str2double(wT.AtomicNumber);
periodictable = ["H" "He" "Li" "Be" "B" "C" "N" "O"];


T = table();
for i = 1:height(wT)
    T.Atom(i) = periodictable(wT.AtomicNumber(i));
    T.X(i) = string(wT.X(i));
    T.Y(i) = string(wT.Y(i));
    T.Z(i) = string(wT.Z(i));
end

end
```